Author Manuscript

Author Manuscript

Author Manuscript

Author Manuscript

HHS Public Access

Author manuscript

Antiviral Res. Author manuscript; available in PMC 2024 April 07.

Published in final edited form as:

Antiviral Res. 2023 January ; 209: 105490. doi:10.1016/j.antiviral.2022.105490.

Tissue replication and mucosal swab detection of Sosuga virus in Syrian hamsters in the absence of overt tissue pathology and clinical disease

Stephen R. Welch[a], **Jana M. Ritter**[b], **Amy J. Schuh**[a], **Sarah C. Genzer**[a], **Teresa E. Sorvillo**[a], **Jessica R. Harmon**[a], **JoAnn D. Coleman-McCray**[a], **Shilpi Jain**[a], **Punya Shrivastava-Ranjan**[a], **Josilene Nascimento Seixas**[b], **Lindsey B. Estetter**[b], **Pamela S. Fair**[b], **Jonathan S. Towner**[a], **Joel M. Montgomery**[a], **César G. Albariño**[a], **Christina F. Spiropoulou**[a], **Jessica R. Spengler**[a,*]

[a]Viral Special Pathogens Branch, Division of High Consequence Pathogens and Pathology, Centers for Disease Control and Prevention, 1600 Clifton Road, Atlanta, GA, 30329, USA

[b]Infectious Diseases Pathology Branch, Division of High Consequence Pathogens and Pathology, Centers for Disease Control and Prevention, 1600 Clifton Road, Atlanta, GA, 30329, USA

Abstract

Human infection with Sosuga virus (SOSV), a recently discovered pathogenic paramyxovirus, has been reported in one individual to date. No animal models of disease are currently available for SOSV. Here, we describe initial characterization of experimental infection in Syrian hamsters, including kinetics of virus dissemination and replication, and the corresponding clinical parameters, immunological responses, and histopathology. We demonstrate susceptibility of hamsters to infection in the absence of clinical signs or significant histopathologic findings in tissues.

Keywords

Sosuga virus; Paramyxovirus; Hamster animal model; Histopathology; Neutralization; Zoonoses

1. Introduction

In 2012, a field researcher developed clinical signs upon returning to the U.S. after 6 weeks of field work in South Sudan and Uganda. The initial clinical presentation included non-specific signs and symptoms (fever, malaise, headache, generalized myalgia and arthralgia, neck stiffness, a metallic taste, and sore throat), but progressed to include a maculopapular rash, several small aphthous soft palate ulcers, mild diarrhea and later, bloody emesis (Albariño et al., 2014). A bone marrow biopsy sample (hospital day 4) showed a mild

*Corresponding author. wsk7@cdc.gov (J.R. Spengler).

Declaration of competing interest

The authors declare that they have no known competing financial interests or personal relationships that could have appeared to influence the work reported in this paper.

Appendix A. Supplementary data

Supplementary data to this article can be found online at https://doi.org/10.1016/j.antiviral.2022.105490.

Author Manuscript Author Manuscript Author Manuscript Author Manuscript

increase in macrocytic hemophagocytosis and pancytopenia with a hypocellular marrow with myeloid hyperplasia and erythroid hypoplasia. When the patient was discharged on hospital day 14, arthralgia and myalgia had improved, oropharynx ulcerations had healed, the rash had resolved without desquamation, and blood counts and hepatic enzyme levels were returning to normal ranges. Considerable sequelae (myalgia, arthralgia, headache, malaise, and fatigue) persisted for several months.

Sosuga virus (SOSV) was identified as the etiologic agent (Albariño et al., 2014), and the virus was later detected in archived bat tissues collected as part of the case-patient's field activities just prior to the onset of clinical signs. SOSV has also been detected in archived Egyptian rousette bat (ERBs: *Rousettus aegyptiacus*) tissues obtained at several other locations in Uganda, indicating that these bats likely serve as a natural SOSV reservoir (Amman et al., 2015). No subsequent cases have been reported. It is not clear if the absence of cases is due to lack of recognition, low pathogenicity or transmissibility of the virus, or if a similar exposure event has yet to be repeated.

Currently, little is known about disease pathogenesis, and no licensed antivirals or vaccines are available. To begin efforts to develop a small animal model of infection, we experimentally infected Syrian hamsters, which are well described models of lethal disease for other high-consequence paramyxoviruses such as Nipah and Hendra virus (Geisbert et al., 2012), and assessed clinical signs, viral replication and dissemination, clinical pathology, serology, and histopathology following infection.

2. Materials and methods

2.1. Biosafety and ethics

All work with infectious virus or infected animals was conducted in a biosafety level 4 (BSL-4) laboratory at the Centers for Disease Control and Prevention (CDC). Experiments involving cDNA encoding viral sequences were performed in accordance with approved Institutional Biosafety Committee protocols. All animal experiments were approved by the CDC Institutional Animal Care and Use Committee and performed in an AAALAC-approved facility.

2.2. Viruses

Generation of recombinant SOSV (rSOSV) and rSOSV expressing the ZsGreen1 (ZsG) reporter gene (rSOSV/ZsG) was previously described (Welch et al., 2018). For these studies, rSOSV (CDC Virharv #814974) and rSOSV/ZsG (CDC Virharv #814975) [both passage 5 (1 × Vero cells followed by 4 × Vero-E6 cells); GenBank: MG812680, MG812681] were grown on Vero-E6 cells infected at MOI 0.01 and harvested 5 days post infection (dpi). Viral titers were determined by $TCID_{50}$ on Vero-E6 cells by immunofluorescence assay: primary antibody was rabbit anti-SOSV NP (Genscript), and secondary antibody was AlexaFluor 594 (Thermo-Fisher); both diluted 1:1,000 in PBS/0.5% w/v BSA. All viral stocks were sequence-verified by next-generation sequencing and confirmed as mycoplasma-free by MycoAlert Plus reagents (Lonza).

Author Manuscript Author Manuscript Author Manuscript Author Manuscript

2.3. Hamster studies

Syrian hamsters (male and female; HsdHan:AURA, Envigo #8903F or #8903M) were group-housed in a climate-controlled laboratory with a 12 h day/night cycle; provided commercially available rodent chow (Teklad Global 18% Protein Rodent Diet) and water *ad libitum*; and housed on autoclaved corn cob bedding (Bed-o'Cobs® ¼", Anderson Lab Bedding) with cotton nestlets in an isolator-caging system (Tecniplast GR900, West Chester, PA, USA) with a HEPA-filtered inlet and exhaust air supply. Microchip transponders (BMDS IPTT-300) were placed sub-cutaneously in the interscapular region for individual identification and to assess body temperature. Insertion sites were closed with GLUture topical tissue adhesive (MWI VETERINARY 034207). Four experimental groups of 20 Syrian hamsters (10 males and 10 females; 5-weeks of age), distributed proportionally by sex, were infected intranasally (IN; 100 μL total, instilled bilaterally) or intraperitoneally (IP; 500 μL total) with 1×10^4 $TCID_{50}$ of rSOSV or rSOSV/ZsG in Dulbecco's Modified Eagle Medium (DMEM, Gibco). Dose was confirmed by back-titer of inoculum preparations. All animals were monitored daily and groups of 4 animals for each experimental group were humanely euthanized at predetermined endpoints (1, 4, 8, 14, 28 dpi). Daily weights, temperatures and clinical scores were recorded for all animals allocated to 14 and 28 dpi endpoints. Terminal intracardiac blood was collected in EDTA or LiH under deep isoflurane anesthesia followed by euthanasia (isoflurane overdose). Mucosal swab specimens were collected immediately post-mortem from oropharynx, genitalia (either intravaginal or preputial), and rectum. Sterile 6" polyester-tipped applicators (Fisher Scientific) were used for oropharyngeal specimens; sterile 6" mini-tip polyester swabs (0.078" tip diameter) with ultra-fine polystyrene handle applicators (Puritan) were used for genital and rectal specimens. Two specimens were collected at each site; one was placed in 500 μL of MagMAX lysis buffer concentrate (Thermo-Fisher Scientific) for RNA isolation and RT-qPCR analysis, and the other in 1 mL of sterile DMEM cell culture media (5% FCS and 2 × antibiotic-antimycotic [Gibco]) for virus isolation and quantification.

2.4. Complete blood count and clinical chemistry

Complete blood counts were performed on whole blood samples collected in EDTA using the VETSCAN HM5 hematology analyzer (Abaxis). Clinical chemistries (Comprehensive Metabolic Panel, Abaxis) was obtained on whole blood collected in lithium heparin and analyzed on Piccolo Xpress chemistry analyzers (Abaxis) within 1 h of collection.

2.5. RT-qPCR

RNA samples were obtained using the MagMAX Pathogen RNA/DNA Kit (RNA eluted in 75 μL; Thermo-Fisher Scientific). Genomic DNA was removed using BaseLine Zero DNase (Epicentre), and RT-qPCR was performed using SuperScript III Platinum One-Step RT-qPCR Kit (Invitrogen) with the following primers and probe detecting the SOSV N gene as previously described (Amman et al., 2015, 2020): PMX-2012 FOR3 - GAT TCG AAC CGG GAA CAT AC; PMX-2012 REV3 - TGG GAT ATC ATC TGC CAT TTC; PMX-2012 PRB3 - FAM-TGC AAG AAC/ZEN/ACC GCT GAC AGT AGG-IABkFQ (IDT). For tissue specimens, approximately 100 mg was placed in 2 mL grinding vials (OPS Diagnostics) with 1 mL of MagMax lysis buffer concentrate and homogenized. Each extraction used 250

Author Manuscript Author Manuscript Author Manuscript Author Manuscript

µL of tissue lysate with 150 µL of 100% isopropanol. Blood samples (50 µL; whole, EDTA) were added to 500 µL of MagMax lysis buffer concentrate and RNA was extracted from 250 µL of lysate as described for the tissue specimens. RT-qPCR results were normalized using 18s rRNA levels (18s rRNA primer/probe assay; Applied Bio-systems) according to the manufacturer's instructions. For RNA quantification, relative SOSV $TCID_{50}$/mL values were interpolated from standard curves generated from serial 10-fold dilutions of SOSV stock of known titer ($TCID_{50}$/mL) in DMEM. These SOSV dilutions were then added to blood, tissue (calf liver) homogenate, or DMEM in volumes identical to those used for collecting experimental blood, tissues, and swab samples. The standard curve for swab samples was based on a calculation in which 20 µL of virus solution was absorbed by the swab applicator.

2.6. Virus isolation and titration of mucosal swab specimens

For virus isolation from mucosal swab specimens, 100 µL of 1 mL original specimen collection volume was added to Vero-E6 cells in 12-well plates and incubated for 7 days before cells were fixed and stained for SOSV protein: primary antibody was rabbit anti-SOSV NP (Genscript), and secondary antibody was AlexaFluor 488 (Thermo-Fisher); both diluted 1:1,000 in PBS/0.5% w/v BSA. For virus titration, 100 µL of specimen was added in 10-fold dilution series (dilution range tested was −1 to −6) on Vero-E6 cells. Immunofluorescence staining was performed as detailed above to calculate $TCID_{50}$ titers (Reed and Muench, 1938).

2.7. Enzyme-linked immunosorbent assay

Plasma samples were tested by indirect enzyme-linked immunosorbent assay (ELISA) for the presence of IgG antibodies reactive to SOSV using a non-recombinant, infectious based virus antigen lysate (Amman et al., 2020) and an uninfected control antigen lysate that were prepared as previously described (Macneil et al., 2011). Wells of 96-well enzyme-linked immunosorbent assay (ELISA) plates were coated (100 µL) with a 1:500 dilution of SOSV lysate (diluent: PBS/1% v/v thimerosal) and corresponding wells were coated with an equivalent dilution of uninfected control lysate. After incubation overnight at 4 °C, the plates were washed with PBS/0.1% v/v Tween-20 (PBS-T) and 100 µL of serum diluent (PBS containing 5% w/v skim-milk and 0.1% v/v Tween-20) was added to each well of the plate. After 10 min, 33 µL of 21:521 dilutions of gamma-irradiated Syrian hamster plasma samples (diluent: PBS containing 5% w/v skim milk powder, 0.5% v/v Tween-20, 1% v/v thimerosal) were added to the first well of the plates and 4-fold serial dilutions, ranging from 1:100 to 1:6,400, were performed. Following a 1 h incubation at 37 °C, the plates were washed with PBS-T and 100 µL of a 1:20,000 dilution of goat anti-Syrian hamster IgG-heavy and light chain cross-adsorbed antibody conjugated to horseradish peroxidase (Bethyl Laboratories) in serum diluent was added to the plates. The manufacturer notes that this antibody reacts specifically with Syrian hamster IgG and with light chains common to other Syrian hamster immunoglobulins. After incubation for 1 h at 37 °C, the plates were washed with PBS-T, 100 µL of the Two-Component ABTS Peroxidase System (KPL) added, and plates were allowed to incubate for 30 min at 37 °C. The plates were then read on a microplate spectrophotometer set at 410 nm. To negate non-specific background reactivity, adjusted OD values were calculated by subtracting the ODs at each four-fold dilution of

Author Manuscript Author Manuscript Author Manuscript Author Manuscript

wells coated with uninfected control antigen lysate from ODs at corresponding wells coated with SOSV lysate. Adjusted sum OD values were determined by summing the adjusted OD values at each four-fold serial dilution. The cut-off value for seropositivity (0.22) was determined by calculating the mean adjusted sum OD value plus 5 standard deviations of 80 plasma collected from SOSV-naïve Syrian hamsters. A hamster with an adjusted sum OD value ≥ 0.22 was considered to have been infected with SOSV and seroconverted with a confidence level >99.99999%.

2.8. Neutralization assay

Neutralization activity of sera from infected animals were measured using a standard protocol in Vero-E6 cells. Briefly, serial five-fold dilutions of sera (150 μL) made in DMEM, were mixed with an equal volume of rSOSV/ZsG containing 100 $TCID_{50}$ (Welch et al., 2018). After incubation at 37 °C for 1 h, 50 μL of virus-serum mixture was inoculated onto Vero-E6 cells in 96 well plates (Cell Carrier Ultra plates, Perki-nElmer) seeded the day before at 1.5×10^4 cells per well. The culture was incubated at 37 °C for 72 h, after which fluorescence intensity was determined using a BioTek Synergy reader (height 6 mm; 100 gain/-sensitivity). Fluorescence readings from quadruplicate wells at each serum concentration were taken. Background signals (no virus) were deducted from fluorescence readings, and data presented as relative to no serum-virus only control. GraphPad Prism was used to generate concentration–response plots. Either a four- or three-parameter equation was used to fit semi-log plots of the data and derive the Neut50 titers.

2.9. Histopathology, immunohistochemistry, and in situ hybridization

Representative sections of brain, heart, lung, liver, spleen, kidney, adrenal gland, eye, trachea, esophagus, parotid salivary gland, lacrimal gland, reproductive tissues, stomach, small intestine, colon, pancreas, and mesenteric lymph nodes, as available, were evaluated by histopathology. Necropsy tissues were fixed in 10% neutral buffered formalin and gamma-irradiated (5×10^6 rad) and processed for routine paraffin histology. Sections were cut at 4 μm, mounted on glass slides, and stained with hematoxylin-eosin for histopathologic evaluation. Un-stained tissue sections processed in the same way were used for immunohistochemical and in situ hybridization studies. IHC assay for Sosuga virus was performed using a rabbit polyclonal antibody raised against Sosuga NP (GenScript), purified by Protein A at 1:2,000 dilution. Un-stained slides were deparaffinized and rehydrated, then subjected to heat induced epitope retrieval (HIER) with citrate buffer (Reveal, Biocare Medical) performed on the Biocare NxGen decloaker (110 °C for 15 min). Anti-Sosuga antibody was applied to the tissue sections and incubated at room temperature for 30 min. Colorimetric detection of attached antibodies was performed using the Mach 4 AP Polymer kit (Biocare Medical) with a Permanent Red Chromogen (Cell Marque/ Millipore Sigma). Slides were counterstained in Mayer's hematoxylin (Polyscientific) and then coverslipped with aqueous mounting medium (Polysciences Inc.). FFPE cell block transfected with NP plasmic served as positive control, and normal rabbit serum in place of primary antibody served as negative control. To localize Sosuga virus RNA in FFPE tissues, an ISH assay using RNAscope negative sense probes targeting the positive sense cRNA SOSV NP sequence (https://www.ncbi.nlm.nih.gov/nuccore/KF774436.1; Advanced Cell Diagnostics, Newark, California; V-SOSV-NP, #573561) was performed as previously

Author Manuscript Author Manuscript Author Manuscript Author Manuscript

described (Bhatnagar et al., 2021; Wang et al., 2012). An FFPE cell block transfected with NP plasmid served as the positive control and tissues not treated with probe served as the negative controls.

2.10. Data analysis and graphics

All graphs were created in GraphPad Prism (v9.4.1). Significance for CBC, clinical chemistry and ELISA were calculated using multiple unpaired *t*-tests. Study schematic was created with BioRender.com.

3. Results

3.1. SOSV disseminates and replicates in Syrian hamsters in the absence of clinical signs

Eighty hamsters (five-week-old males and females; Envigo) were divided equally by sex into experimental groups of 20. This age was chosen as, in our hands, older hamsters (approximately ≥10 weeks old), are more resistant to severe or lethal forms of Nipah paramyxovirus disease. Each group was inoculated intranasally (IN) or intraperitoneally (IP) with either recombinant wild-type virus (rSOSV) or a comparable recombinant ZsG-expressing reporter virus (rSOSV/ZsG), both based on the viral sequence obtained from the patient (Welch et al., 2018). A subset of animals (n = 4, per experimental group) was serially euthanized at 1, 4, 8, 14 and 28 days post infection [dpi] (Fig. 1A). The timepoints were selected to adequately cover the study period and encompass timing post-infection when virus replication, histopathology and clinical disease has been described for Nipah and Hendra paramyxoviruses (DeBuysscher et al., 2013; Genzer et al., 2020; Rockx et al., 2011; Welch et al., 2022). Blood, plasma, tissues, and mucosal swab specimens were collected for clinical, virological, histological, and immunological analyses at each timepoint.

Weight and body temperature were recorded daily in animals euthanized at 14 and 28 dpi. No clinical signs of infection were apparent throughout the infection period, and all animal survived until predetermined end-points (up to 28 dpi; Fig. 1B) with no notable changes in body weight or temperature observed (Fig. 1C). However, viral RNA (vRNA) was detected transiently in the majority of tissues and swab samples (Fig. 1D), indicating subclinical infection. In general, vRNA kinetics varied by inoculation routes but not between rSOSV and rSOSV/ZsG infected animals: vRNA was found in a broader range of tissue types and as early as 1 dpi in IP-inoculated animals, whereas vRNA was not observed in most tissues until 4 dpi in IN-inoculated animals. Independent of inoculation route, vRNA levels were transient; at >8 dpi vRNA was limited to select tissues including lung (only 1 IN-inoculated animal at 14 dpi) and spleen. The only tissue with observable vRNA at study completion (28 dpi) was spleen (4 of 8 for IN; 8 of 8 for IP). vRNA detection in oral swabs was most prominent in terms of frequency and titer in IN-inoculated hamsters, whereas rectal swab detection was more frequent in IP-inoculated hamsters. No infectious virus could be isolated from swab samples.

Consistent with the absence of clinical signs, there was minimal evidence of SOSV-associated alterations in clinical chemistry and hematology analytes. The only change of

Author Manuscript Author Manuscript Author Manuscript Author Manuscript

note was the presence of leukocytosis with neutrophilia that predominates the hemogram at early timepoints (1 and 4 dpi), consistent with inflammatory responses and is presumably virus-associated (Fig. 2). Other differences are likely due to age-associated changes, including increasing albumin and total protein levels, decreasing alkaline phosphatase levels; and increasing RBC, hemoglobin, and hematocrit (Fig. 2, Fig. S1).

3.2. Hamsters seroconvert and generate neutralizing antibodies to SOSV infection

Hamsters euthanized at 1 (mean adjusted sum OD: −0.03, SD: 0.02) and 4 dpi (mean adjusted sum OD: −0.06, SD: 0.01) did not generate detectable SOSV IgG antibody responses (Fig. 3A). SOSV IgG antibody responses markedly increased between 8 and 28 dpi, with 13 of 16 (81.3%) hamsters seroconverting by 8 dpi (mean adjusted sum OD = 1.08, SD = 0.81), 16 of 16 (100.0%) hamsters seroconverting by 14 dpi (mean adjusted sum OD = 4.38, SD = 0.63), and 16 of 16 (100.0%) hamsters by 28 dpi (mean adjusted sum OD = 7.14, SD = 0.65). At 8 dpi, anti-SOSV IgG antibody responses were significantly higher ($p = 0.0003$) in hamsters inoculated by the IP route (mean adjusted sum OD = 1.60, SD = 0.70) compared to hamsters inoculated by the IN route (mean adjusted sum OD = 0.55, SD = 0.54). No significant differences were seen between inoculation routes at subsequent time-points or between rSOSV and rSOSV/ZSG at any timepoint. Furthermore, 28 dpi plasma samples were evaluated for neutralizing activity (50% neutralization titers [Neut50]); all samples demonstrated similar levels of neutralizing antibodies independent of virus and inoculation route, with a geometric mean titer Neut50 across all groups of 1617 (Fig. 3B, Fig. S2).

3.3. Intranasally-inoculated SOSV causes minimal, transient lung pathology in hamsters

Histopathologic evaluation of tissues was performed for all hamsters euthanized at 4 dpi for both rSOSV- and rSOSV/ZsG-infected groups; 4 dpi was chosen based on most consistent and widespread detection of virus by RT-qPCR at this timepoint. At this time point, no histopathologic differences were seen between the rSOSV- and rSOSV/ZsG-infected animals. Therefore, tissues from later timepoints (8, 14 and 28 dpi) were evaluated for rSOSV-infected hamsters only. In addition, to investigate potential virus-associated pathology after peak viral load, lung and liver were evaluated for all study animals at all timepoints.

Parenchymal collapse precluded optimal assessment of lungs for interstitial inflammation; however, a subset of lungs at all timepoints and for both routes had patchy foci of increased interstitial cellularity, including few neutrophils (Fig. 4A). This change was most prominent in the lungs of IN-inoculated hamsters at 4 dpi (5 of 8) and 8 dpi (7 of 8). Additionally, for IN-inoculated hamsters, one each at 1 dpi and 4 dpi had a single focus of acute bronchopneumonia, although this may be independent of virus infection as a result of IN-inoculation alone (Forero et al., 2022). At 8 dpi, 5 of 8 IN-inoculated hamsters had foci of type II pneumocyte or bronchiolar epithelial proliferation associated with mononuclear to mixed inflammation and apoptotic debris (Fig. 4B). Proliferative epithelial cells showed reactive atypia (karyocytomegaly, vesicular nuclei, prominent nucleoli, and occasional multinucleation) (Fig. 4C); no viral inclusions were seen. An early stage of this lesion without epithelial proliferation was minimally apparent in 3 of 8 IN-inoculated hamsters at

Author Manuscript Author Manuscript Author Manuscript Author Manuscript

4 dpi; it was not present at other timepoints for IN-inoculated hamsters or in lungs from any IP-inoculated hamster. Five animals (one 4 dpi IP-inoculated, two 14 dpi IN-inoculated, and two 28 dpi IN-inoculated) had focal, minimal, mononuclear infiltrates around parotid salivary ducts. Glycogen content in centrilobular zones of livers varied within all groups. No other significant histopathologic alterations were seen.

3.4. In situ hybridization localizes SOSV RNA primarily to lung and lymphoid tissues

RNAscope in situ hybridization (ISH) and immunohistochemistry (IHC), both targeting SOSV NP, were evaluated for utility in assessing virus distribution in tissues. ISH and IHC revealed a similar distribution of viral RNA and antigen, respectively. ISH showed more intense and abundant staining than IHC during initial testing; ISH was therefore subsequently exclusively used for determining virus distribution in tissues. ISH was performed on all tissues from all hamsters sampled at 4 dpi and on select tissues from hamsters sampled at remaining timepoints (Fig. 4D–J). Staining was detected in a subset of tissues in IN- and IP-inoculated animals; patterns were route-associated and did not differ between virus inoculum (rSOSV or rSOSV/ZsG). Overall, detection was restricted to lung and lymphoid tissues (mucosa-associated lymphoid tissue, spleen, mesenteric lymph node).

In IN-inoculated animals, ISH staining was predominantly in respiratory tissues, with limited evidence of dissemination to intestinal lymphoid tissues. At 4 dpi, 7 of 8 IN-inoculated hamsters had multifocal staining in lung tissue (Fig. 4D); extent in individual animals generally correlated with level of viral load as determined by corresponding fresh tissue RT-qPCR. Staining was somewhat clustered around terminal airways and often localized within bronchial-associated lymphoid tissue (BALT) [Fig. 4E]; no definitive bronchial or bronchiolar epithelial, or vascular endothelial staining was seen. Lungs from 8 dpi with histopathological lesions were also examined by ISH. Rare, punctate staining was associated with inflammatory/epithelial proliferative foci or BALT in these lungs (Fig. 4F). In addition to pulmonary staining, 2 of 8 IN-inoculated hamsters had mesenteric lymph node tissue available from 4 dpi for evaluation; both showed rare staining in lymph node, one of which also had staining in small intestinal gut-associated lymphoid tissue (GALT).

In IP-inoculated animals, staining was detected in limited abdominal viscera and small intestinal GALT. At 4 dpi, 3 of 6 IP-inoculated hamsters had rare staining in splenic white pulp (2 of 8 not available for evaluation; Fig. 4G). Of 5 IP-inoculated hamsters with mesenteric lymph node available, two also had rare staining in lymph node follicles (Fig. 4H). Five of 8 had staining in small intestinal GALT, two of which also had very rare staining within epithelium immediately overlying GALT (Fig. 4I and J). Notably, most GALT staining had a subepithelial distribution, in regions with prominent macrophages.

Finally, additional ISH was performed on select tissues from IN- or IP-inoculated animals (rSOSV and rSOSV/ZsG) at 1, 8, 14 and 28 dpi based on two criteria: presence of minimal, nonspecific histopathologic changes or comparably higher viral load in a tissue than from the same tissue in animals at 4 dpi. A subset of tissues from 10 additional animals were examined, including kidney, brain, eye, salivary gland, spleen, heart, reproductive tract specimens; no staining was seen in any of these additional tissues.

Author Manuscript Author Manuscript Author Manuscript Author Manuscript

4. Discussion

Due to notable public health concerns posed by other highly pathogenic paramyxoviruses, including Nipah and Hendra virus with case fatality rates of 50–80% in humans (Kenmoe et al., 2019; Luby and Gurley, 2012), development of animal models to further study SOSV pathogenesis and identify countermeasures is prudent. We selected Syrian hamsters given their known susceptibility to other paramyxoviruses; both Nipah and Hendra virus cause lethal disease in hamsters and recapitulate both the respiratory and neurological signs reported in humans (Geisbert et al., 2012). These studies confirm the susceptibility of hamsters to SOSV and their utility as an infection model but do not support use of hamsters as a model of severe disease. In the absence of overt clinical signs, IN-inoculation results in lung infection without significant pathology except evidence of transient lesions from IN-inoculated hamsters at 8 dpi. Overall, both IN and IP exposure resulted in virus dissemination and replication, as evidenced by vRNA and ISH detection associated with minimal pathology. vRNA was also detected in mucosal specimens; however, we were unable to isolate infectious virus, suggesting that shedding of infectious virus and corresponding transmission risk would be low.

To date, experimental infection of SOSV has only been described in ERBs, the recognized reservoir host for SOSV (Amman et al., 2020; Kirejczyk et al., 2022). Like ERBs, we found that hamsters seroconvert with no evidence of overt morbidity or mortality, and virus is detected in blood, tissues, and mucosal swab specimens. While the bat studies used subcutaneous inoculation, we selected IN- and IP-inoculation to evaluate the possibility of route-dependent susceptibility, clinical course, and virus dissemination kinetics. Similar to reports for other infection models, kinetics of infection and shedding in hamsters were associated with exposure route (Wozniak et al., 2021), although both resulted in disseminated viral replication and comparable kinetics of seroconversion.

In ERBs, small intestine and salivary glands were the major sites of replication and were associated with tissue changes associated with sparse antigen detection. In bats, GALT staining was in large intestine, whereas in hamsters staining was localized to the small intestinal GALT. Inflammation around salivary ducts with rare staining by IHC was reported in bats, whereas in hamsters there was minimal inflammation around a single duct in only a few animals without staining, likely representing a background lesion unrelated to virus infection. In bats, intestinal villous pathology was reported with IHC staining (Kirejczyk et al., 2022). Significant villous changes were not identified in hamsters from this study; however, superficial mucosal autolysis may have precluded identification of mild epithelial degenerative changes. Finally, lesion scores in bats increased over time and antigen persisted in a subset of tissues, while in hamsters, lesions were absent and virus was not detected by ISH in the subset of tissues tested, suggesting resolution of infection in hamsters over time.

Overall, our data are consistent with reports of variable virus-dependent susceptibility of hamsters to paramyxovirus-associated disease and present similar features of infection as reported in bats. Following IN-inoculation of hamsters with avian paramyxoviruses, all but 1 serotype resulted in mild or inapparent clinical signs; however, pathological changes were noted in pulmonary tissue (Samuel et al., 2011). While we did not observe the overt

Author Manuscript Author Manuscript Author Manuscript Author Manuscript

bronchointerstitial pneumonia reported with avian paramyxoviruses, we did find similar bronchiolar epithelial and pneumocyte proliferation and inflammation associated with virus dissemination to lung parenchyma after IN inoculation. We also showed an apparent tropism of SOSV for lymphoid tissue, with detection in BALT, GALT, and mesenteric lymph node after IN-inoculation, and the addition of spleen after IP-inoculation.

These data provide a basis for further efforts to develop infection and disease models of SOSV for pathogenesis studies and medical countermeasure development. While immunocompetent Syrian hamsters did not demonstrate notable clinical signs, given their susceptibility to infection, future studies may consider use of immunodeficient hamsters, chemically immunosuppressed (Schaecher et al., 2008; Vergote et al., 2017) or knockout strains (Brocato et al., 2020; Gowen et al., 2017; Miao et al., 2018; Ranadheera et al., 2020), to further develop SOSV animal models and to investigate immune contributors to protection.

Supplementary Material

Refer to Web version on PubMed Central for supplementary material.

Acknowledgements

The authors thank Julu Bhatnagar for assistance with in situ hybridization, and Heather Hayes for histology support.

Financial support

This work was supported in part by CDC Emerging Infectious Disease Research Core funds and by an appointment to the Research Participation Program at the Centers for Disease Control and Prevention administered by the Oak Ridge Institute for Science and Education through an interagency agreement between the U.S. Department of Energy and CDC (S.J.).

Data availability

Data will be made available on request.

References

Albariño CG, Foltzer M, Towner JS, Rowe LA, Campbell S, Jaramillo CM, Bird BH, Reeder DM, Vodzak ME, Rota P, Metcalfe MG, Spiropoulou CF, Knust B, Vincent JP, Frace MA, Nichol ST, Rollin PE, Ströher U, 2014. Novel paramyxovirus associated with severe acute febrile disease, South Sudan and Uganda, 2012. Emerg. Infect. Dis 20, 211–216. [PubMed: 24447466]

Amman BR, Albariño CG, Bird BH, Nyakarahuka L, Sealy TK, Balinandi S, Schuh AJ, Campbell SM, Ströher U, Jones MEB, Vodzack ME, Reeder DM, Kaboyo W, Nichol ST, Towner JS, 2015. A recently discovered pathogenic paramyxovirus, Sosuga virus, is present in Rousettus aegyptiacus fruit bats at multiple locations in Uganda. J. Wildl. Dis 51, 774–779. [PubMed: 25919464]

Amman BR, Schuh AJ, Sealy TK, Spengler JR, Welch SR, Kirejczyk SGM, Albariño CG, Nichol ST, Towner JS, 2020. Experimental infection of Egyptian rousette bats (Rousettus aegyptiacus) with Sosuga virus demonstrates potential transmission routes for a bat-borne human pathogenic paramyxovirus. PLoS Neglected Trop. Dis 14, e0008092.

Bhatnagar J, Gary J, Reagan-Steiner S, Estetter LB, Tong S, Tao Y, Denison AM, Lee E, DeLeon-Carnes M, Li Y, Uehara A, Paden CR, Leitgeb B, Uyeki TM, Martines RB, Ritter JM, Paddock CD, Shieh W-J, Zaki SR, 2021. Evidence of severe acute respiratory syndrome Coronavirus 2 replication

Author Manuscript Author Manuscript Author Manuscript Author Manuscript

and tropism in the lungs, airways, and vascular endothelium of patients with fatal Coronavirus disease 2019: an autopsy case series. J. Infect. Dis 223, 752–764. [PubMed: 33502471]

Brocato RL, Principe LM, Kim RK, Zeng X, Williams JA, Liu Y, Li R, Smith JM, Golden JW, Gangemi D, Youssef S, Wang Z, Glanville J, Hooper JW, 2020. Disruption of adaptive immunity enhances disease in SARS-CoV-2-infected Syrian hamsters. J. Virol 94.

DeBuysscher BL, de Wit E, Munster VJ, Scott D, Feldmann H, Prescott J, 2013. Comparison of the pathogenicity of Nipah virus isolates from Bangladesh and Malaysia in the Syrian hamster. PLoS Neglected Trop. Dis 7.

Forero C, Ritter JM, Seixas JN, Coleman-McCray JD, Brake M, Condrey JA, Tansey C, Welch SR, Genzer SC, Spengler JR, 2022. Volume-Associated Clinical and Histopathological Effects of Intranasal Instillation in Syrian Hamsters: Considerations for Infection and Therapeutic Studies, 11. Pathog., Basel, Switzerland.

Geisbert TW, Feldmann H, Broder CC, 2012. Animal challenge models of henipavirus infection and pathogenesis. Curr. Top. Microbiol. Immunol 359, 153–177. [PubMed: 22476556]

Genzer SC, Welch SR, Scholte FEM, Harmon JR, Coleman-McCray JD, Lo MK, Montgomery JM, Nichol ST, Spiropoulou CF, Spengler JR, 2020 May 11. Alterations in Blood Chemistry Levels Associated With Nipah Virus Disease in the Syrian Hamster Model. J Infect Dis. 221 (Suppl 4), S454–S459. 10.1093/infdis/jiz552. [PubMed: 31747016]

Gowen BB, Westover JB, Miao J, Van Wettere AJ, Rigas JD, Hickerson BT, Jung K-H, Li R, Conrad BL, Nielson S, Furuta Y, Wang Z, 2017. Modeling severe fever with thrombocytopenia syndrome virus infection in golden Syrian hamsters: importance of STAT2 in preventing disease and effective treatment with Favipiravir. J. Virol 91.

Kenmoe S, Demanou M, Bigna JJ, Nde Kengne C, Fatawou Modiyinji A, Simo FBN, Eyangoh S, Sadeuh-Mba SA, Njouom R, 2019. Case fatality rate and risk factors for Nipah virus encephalitis: a systematic review and meta-analysis. J. Clin. Virol 117, 19–26. [PubMed: 31132674]

Kirejczyk SGM, Amman BR, Schuh AJ, Sealy TK, Albariño CG, Zhang J, Brown CC, Towner JS, 2022. Histopathologic and immunohistochemical evaluation of induced lesions, tissue tropism and host responses following experimental infection of Egyptian rousette bats (Rousettus aegyptiacus) with the zoonotic paramyxovirus. Sosuga Virus. Viruses 14.

Luby SP, Gurley ES, 2012. Epidemiology of henipavirus disease in humans. Curr. Top. Microbiol. Immunol 359, 25–40. [PubMed: 22752412]

Macneil A, Reed Z, Rollin PE, 2011. Serologic cross-reactivity of human IgM and IgG antibodies to five species of Ebola virus. PLoS Neglected Trop. Dis 5, e1175.

Miao J, Ying B, Li R, Tollefson AE, Spencer JF, Wold WSM, Song S-H, Kong I-K, Toth K, Wang Y, Wang Z, 2018. Characterization of an N-terminal non-core domain of RAG1 gene disrupted Syrian hamster model generated by CRISPR Cas9. Viruses 10.

Ranadheera C, Valcourt EJ, Warner BM, Poliquin G, Rosenke K, Frost K, Tierney K, Saturday G, Miao J, Westover JB, Gowen BB, Booth S, Feldmann H, Wang Z, Safronetz D, 2020. Characterization of a novel STAT 2 knock-out hamster model of Crimean-Congo hemorrhagic fever virus pathogenesis. Sci. Rep 10, 12378. [PubMed: 32704046]

Reed LJ, Muench H, 1938. A simple method for estimating fifty percent endpoints. Am. J. Hyg 27, 493–497.

Rockx B, Brining D, Kramer J, Callison J, Ebihara H, Mansfield K, Feldmann H, 2011. Clinical outcome of henipavirus infection in hamsters is determined by the route and dose of infection. J. Virol 85, 7658–7671. [PubMed: 21593160]

Samuel AS, Subbiah M, Shive H, Collins PL, Samal SK, 2011. Experimental infection of hamsters with avian paramyxovirus serotypes 1 to 9. Vet. Res 42, 38. [PubMed: 21345199]

Schaecher SR, Stabenow J, Oberle C, Schriewer J, Buller RM, Sagartz JE, Pekosz A, 2008. An immunosuppressed Syrian golden hamster model for SARS-CoV infection. Virology 380, 312–321. [PubMed: 18760437]

Vergote V, Laenen L, Vanmechelen B, Van Ranst M, Verbeken E, Hooper JW, Maes P, 2017. A lethal disease model for New World hantaviruses using immunosuppressed Syrian hamsters. PLoS Neglected Trop. Dis 11, e0006042.

Author Manuscript Author Manuscript Author Manuscript Author Manuscript

Wang F, Flanagan J, Su N, Wang L-C, Bui S, Nielson A, Wu X, Vo H-T, Ma X-J, Luo Y, 2012. RNAscope: a novel in situ RNA analysis platform for formalin-fixed, paraffin-embedded tissues. J. Mol. Diagn 14, 22–29. [PubMed: 22166544]

Welch Stephen R., Chakrabarti AK, Wiggleton Guerrero L, Jenks HM, Lo MK, Nichol ST, Spiropoulou CF, Albariño CG, 2018. Development of a reverse genetics system for Sosuga virus allows rapid screening of antiviral compounds. PLoS Neglected Trop. Dis 12, e0006326.

Welch SR, Spengler JR, Harmon JR, Coleman-McCray JD, Scholte FEM, Genzer SC, Lo MK, Montgomery JM, Nichol ST, Spiropoulou CF, 2022. Defective interfering viral particle treatment reduces clinical signs and protects hamsters from lethal Nipah virus disease. mBio 13, e0329421. [PubMed: 35297677]

Wozniak DM, Riesle-Sbarbaro SA, Kirchoff N, Hansen-Kant K, Wahlbrink A, Stern A, Lander A, Hartmann K, Krasemann S, Kurth A, Prescott J, 2021. Inoculation route-dependent Lassa virus dissemination and shedding dynamics in the natural reservoir - Mastomys natalensis. Emerg. Microb. Infect 10, 2313–2325.

Author Manuscript Author Manuscript Author Manuscript Author Manuscript

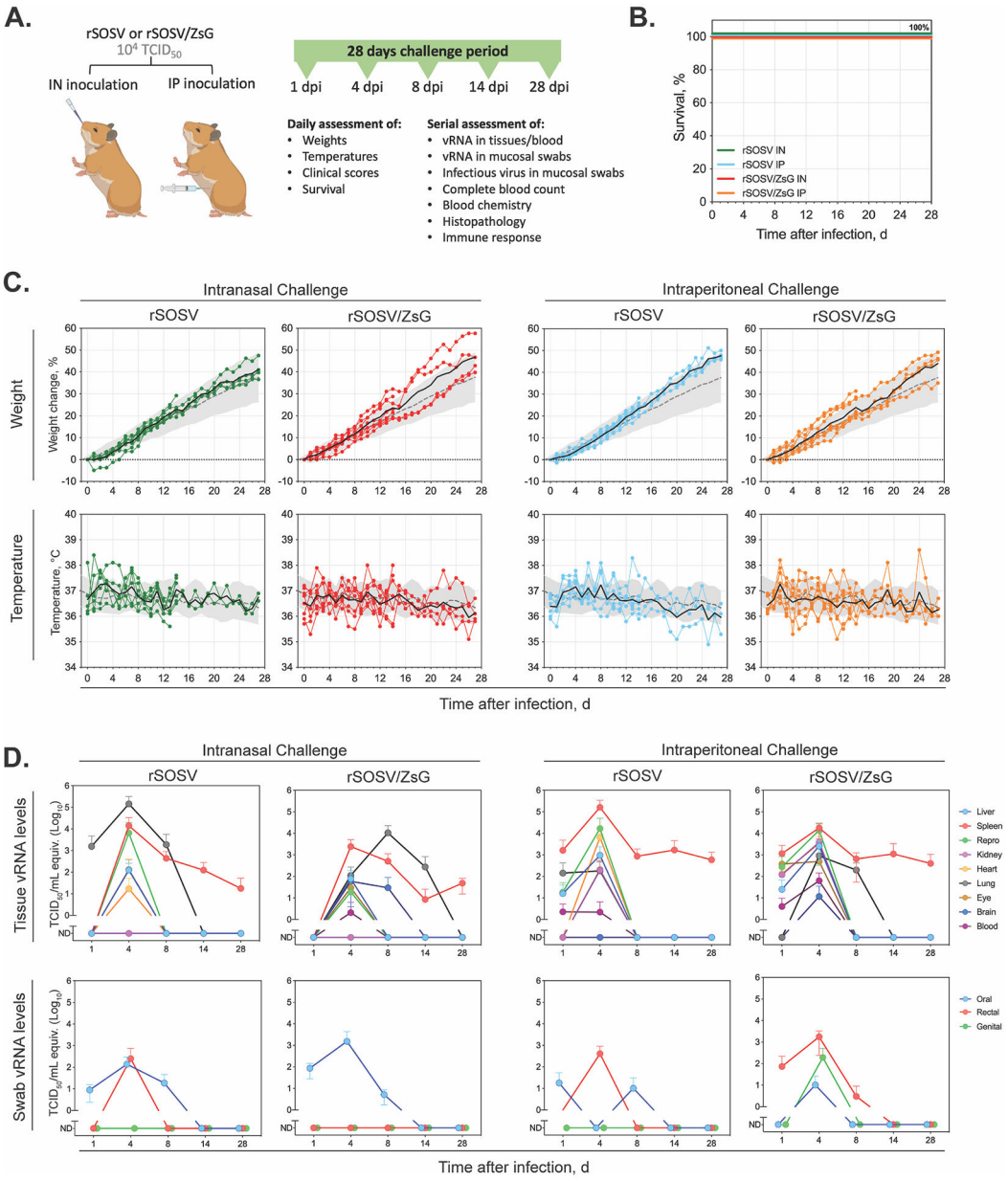

Fig. 1. Clinical and virological assessment of Sosuga virus-infected Syrian hamsters.

(A) Study overview and timeline. Syrian hamsters were infected intranasally (IN) or intraperitoneally (IP) with recombinant SOSV (rSOSV or rSOSV/ZsG; n = 20 per experimental group; dose = 1×10^4 $TCID_{50}$). Four hamsters from each experimental group were serially euthanized at one of five predetermined time-points (1, 4, 8, 14, and 28 days post infection (dpi)). (B) Kaplan-Meier curves showing survival (C) Weight change (% from baseline at 0 dpi) and body temperatures, dots represent individual animals, and solid black lines represent the experimental group mean. Also represented are historical uninfected control data for weights and temperatures of age-matched Syrian hamsters (n = 39, 15 male and 24 female): grey dashed line representing the mean and grey shaded area the standard deviation. (D) Viral RNA (vRNA) from samples collected at the time of euthanasia (1, 4, 8,

14, or 28 dpi). vRNA levels were quantified in blood, tissues (liver, spleen, gonad [ovary or testicle], kidney, heart, lung, eye, and brain), and mucosal swabs (oral, rectal, and genital). Dots represent experimental mean (n = 4), and error bars the standard deviation.

Author Manuscript Author Manuscript Author Manuscript Author Manuscript

Author Manuscript Author Manuscript Author Manuscript Author Manuscript

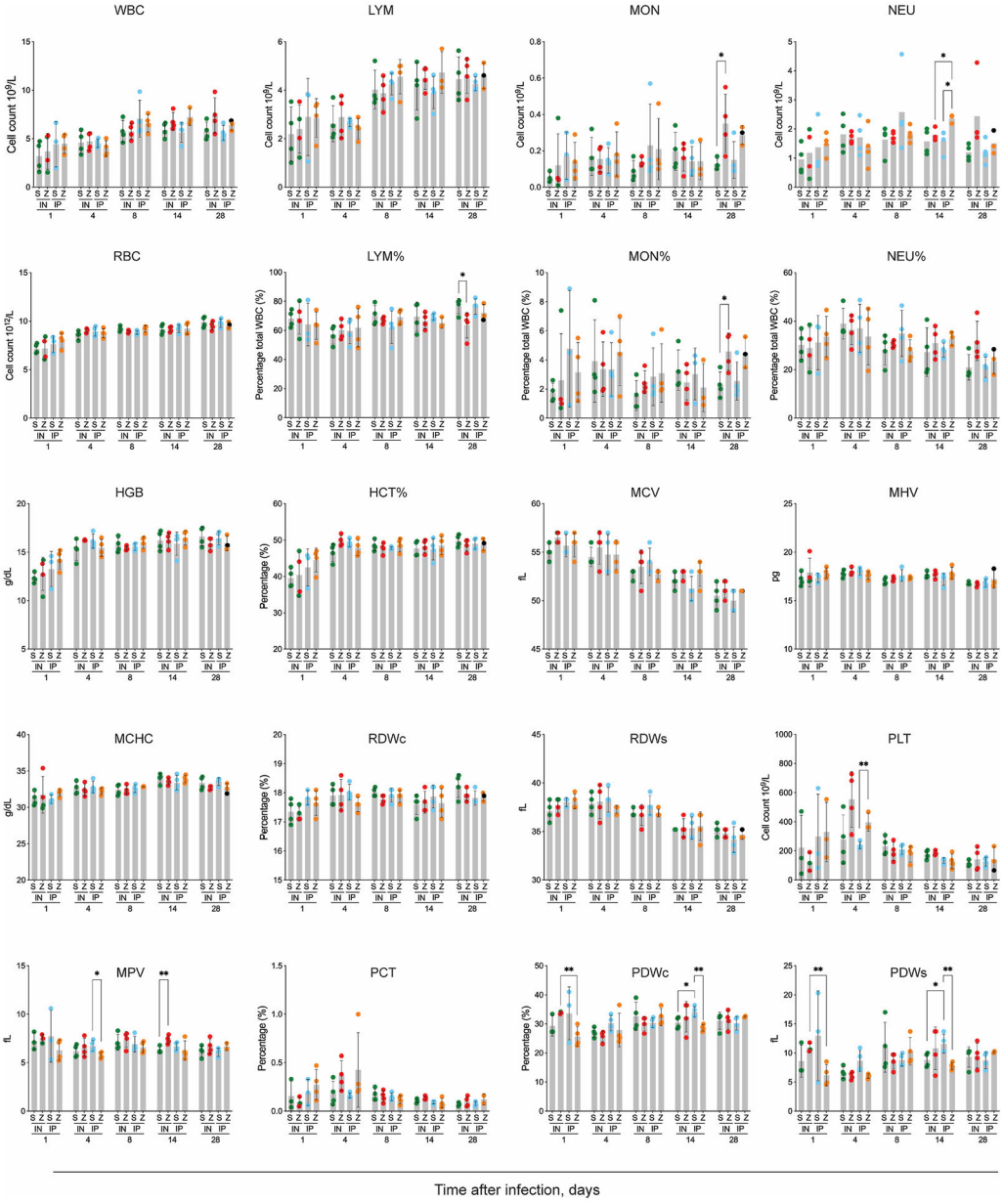

Fig. 2. Complete blood count analytes from Sosuga virus-infected Syrian hamsters.

CBC analyses were run on EDTA whole blood samples obtained from Sosuga virus-infected Syrian hamsters at indicated day post-infection (1, 4, 8, 14, or 28). S, rSOSV; Z, rSOSV/ZsG; IN, intranasal; IP, intraperitoneal. WBC, white blood cell count; LYM, lymphocyte; MON, monocyte; NEU, neutrophil; RBC, red blood cell; HCT, hematocrit; HGB, Hemoglobin; MCV, mean corpuscular volume; MCH, mean corpuscular hemoglobin; MCHC, mean corpuscular hemoglobin concentration; RDWc, red cell distribution width coefficient of variation; RDWs, red cell distribution width standard deviation, PLT, platelet count; MPV, mean platelet volume; PCT, plateletcrit; PDWc, platelet distribution width coefficient of variation; PDWs, platelet distribution width standard deviation. Significance

Author Manuscript Author Manuscript Author Manuscript Author Manuscript

calculated by unpaired *t*-test, controlled for false discovery rate by two-stage step-up (Benjamini, Krieger, and Yekutieli): ✱✱, p = <0.01; ✱, p = <0.05.

Author Manuscript Author Manuscript Author Manuscript Author Manuscript

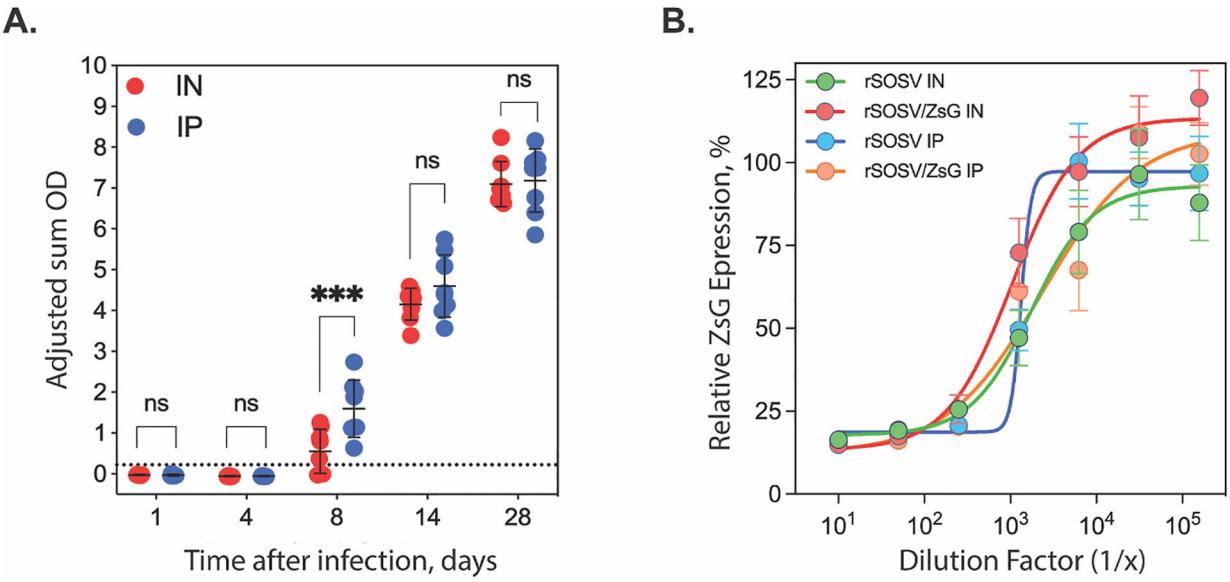

Fig. 3. Sosuga virus serology in experimentally infected Syrian hamsters.

(A) ELISA detection of anti-SOSV IgG levels in plasma of rSOSV-inoculated hamsters (both rSOSV and rSOSV/ZsG) separated by inoculation route (IN, intranasal; IP, intraperitoneal) at 1, 4, 8, 14, and 28 days post infection. Significance calculated by unpaired *t*-test: ***, p = <0.001; ns, not significant. Dashed horizontal line represents the cutoff value for seropositivity (0.22). (B) Plasma from hamsters at 28 days post infection [by virus (rSOSV and rSOSV/ZsG) and inoculation route (IN, intranasal; IP, intraperitoneal)], was evaluated for neutralizing activity calculated as mean 50% neutralization titers (Neut50). Dots represent experimental mean (n = 4), and error bars the standard error mean.

Author Manuscript Author Manuscript Author Manuscript Author Manuscript

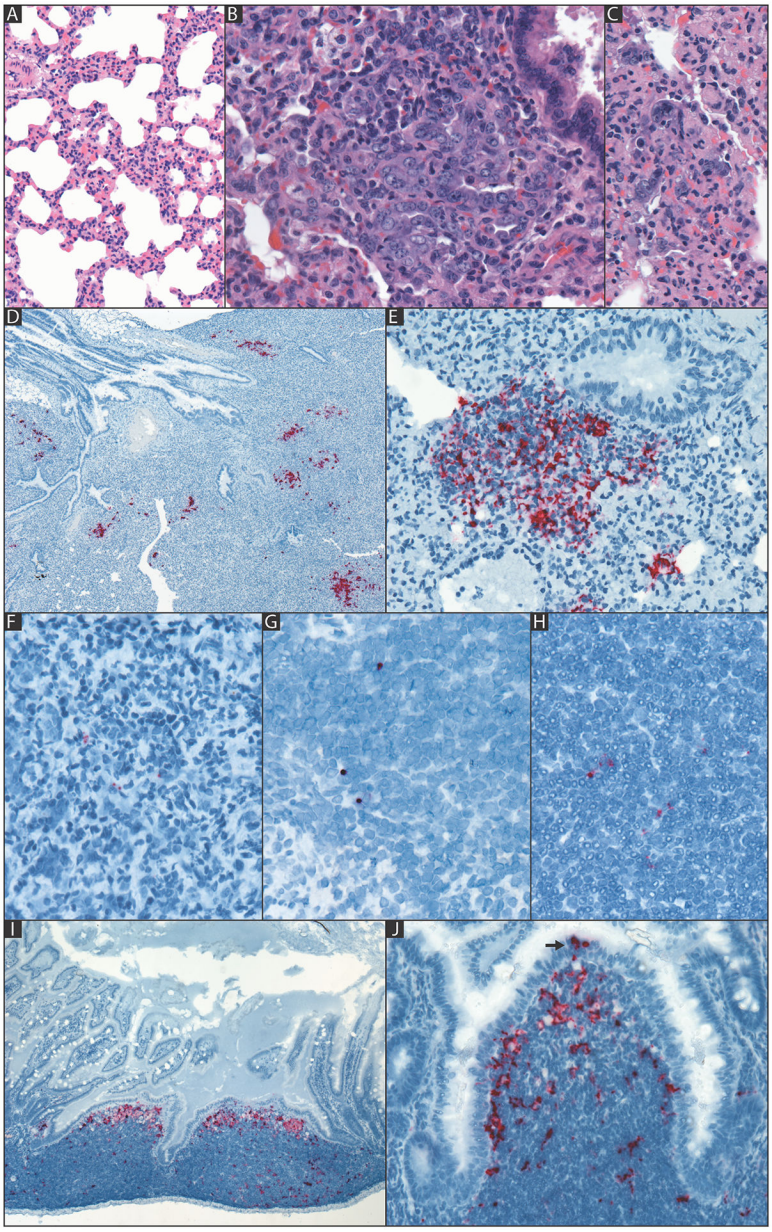

Fig. 4. Sosuga virus-associated lung pathology and viral RNA localization by in situ hybridization (ISH) in intranasally (A–F) or intraperitoneally (G–J) inoculated hamsters.

(A) Mild pulmonary interstitial expansion by inflammatory cells at 4 dpi. (B) Focus of type II pneumocyte hyperplasia and mononuclear inflammatory cells at 8 dpi. (C) Epithelial cells with reactive atypia, including karyocytomegaly and multinucleation, 8 dpi. (D) Lung with widespread, patchy SOSV staining by ISH in the lung parenchyma of a 4 dpi IN-inoculated hamster. There is no staining of bronchial or bronchiolar epithelium. (E) Prominent staining within bronchial-associated lymphoid tissue (BALT) at 4 dpi. (F) Rare SOSV staining in a focus of pulmonary inflammation in an 8 dpi IN-inoculated hamster. (G–H) Rare SOSV staining in the spleen (G), and mesenteric lymph node (H) of 4 dpi IP-inoculated hamsters. (I) SOSV staining in the small intestinal gut-associated lymphoid tissue (GALT) from a 4 dpi IP-inoculated hamster. Staining is concentrated in the subepithelial region of lymphoid

follicles; there is no staining of intestinal epithelium. (J) Rare staining within intestinal epithelial cells (arrow) overlying GALT with staining.

Author Manuscript Author Manuscript Author Manuscript Author Manuscript